



# Domain adaptation for structural health monitoring via physics-informed and self-attention-enhanced generative adversarial learning

Liangfu Ge, Ayan Sadhu \*

Department of Civil and Environmental Engineering, The Western Academy for Advanced Research, Western University, London, ON N6A 3K7, Canada



## ARTICLE INFO

Communicated by Dervilis Nikolaos

**Keywords:**

Structural health monitoring  
Domain adaptation  
Self-attention  
Physical constraint  
Generative adversarial learning

## ABSTRACT

Health monitoring technologies, empowered by sensor-driven information and model updating, play an important role in assessing the status of civil structures and detecting anomalies. However, significant domain discrepancies exist in the distribution of physical parameters between numerical structural models and their real-world counterparts. As a result, many health monitoring theories struggle to be effective in practice, even if they perform perfectly in the simulated data. To bridge the domain discrepancies, this paper proposes an unsupervised domain adaptation approach based on an adapted cycle-consistent generative adversarial network (CycleGAN) that incorporates physical constraints and a self-attention mechanism. The approach focuses on the mutual transformation of the multi-channel time series obtained from numerical models and actual structures. Specifically, the physical constraints are derived from the governing equation of linear dynamic systems, while the self-attention mechanism is achieved by adding transformer structures to both the generator and discriminator. Through free-vibration experiments on a steel beam and a large-scale steel bridge model, the physical constraints and transformer structures have proven beneficial for improving the learning capability and training stability of the GAN model. Furthermore, the proposed approach is not only verified as effective in transforming acceleration responses between the test structures and their corresponding finite element models in both time and frequency domains but has also been shown to reproduce mode shapes accurately.

## 1. Introduction

Structural health monitoring (SHM) is an essential technology for the safety management of infrastructure, which helps to discover structural anomalies in time and significantly reduces maintenance costs. Data from field measurement is the premise of SHM, but in many cases, obtaining sufficient data from the real structure, especially for large-scale structures, can be labor-intensive and expensive. With these practical challenges, simulations are frequently employed, offering insights into potential structural behaviors across various scenarios. However, a notable challenge in practical SHM implementation is that the simulation data obtained by various theoretical models exhibits unpredictable discrepancies when compared with the measurements from actual structures, i.e., domain drifts. The domain drifts between simulation and real-world measurement often stem from modeling simplifications, variability in

\* Corresponding author.

E-mail addresses: [lge25@uwo.ca](mailto:lge25@uwo.ca) (L. Ge), [asadhu@uwo.ca](mailto:asadhu@uwo.ca) (A. Sadhu).

material properties, and impacts of the operating environment. Historically, model updating techniques have been favored to bridge these domain drifts for their clear physical interpretation. Model updating approaches such as the response surface method [1], sensitivity-based method [2] and Bayesian updating [3] have been reported to have great success in real bridge tests. However, they still have some limitations. Specifically, the updating process, which often requires iterative optimization, can become computationally intensive as the complexity of structures increases. Also, when dealing with complex parameter spaces with limited experimental data, these methods possibly get trapped in local optima, resulting in poor generalization ability to new scenarios.

Deep learning techniques [4–11], which have recently garnered increasing attention due to exceptional robustness and generalization capability to real-world applications, provide another choice to cope with domain drifts of simulation and measurement. These approaches mostly adopt the strategy of exploring the parameter space in simulations, subsequently using the simulated data to train the latent mapping between observed responses and structural parameters. For instance, Yuan et al. [12] trained a generative adversarial network (GAN) with simulated acceleration responses of a steel-concrete bridge tower under various combinations of structural parameters. The trained GAN was used to predict the structural parameter with the measured acceleration as input. Teng et al. [13] generated digital twin models and their responses to random excitation force with different parameter distributions for the training of a damage classification convolutional neural network (CNN). Subsequently, they employed transfer learning to count damages on a steel truss bridge. Zhang and Sun [14] proposed a physics-informed neural network (PINN) that trained with simulated data from various damage scenarios and successfully applied it to the damage localization of a three-story frame structure. Recently, they also employed transfer learning to obtain prior knowledge of damages and guided Bayesian mode updating to achieve damage identification in a five-story frame structure [15]. Similarly, Wang et al. [16] successfully detected damages in a frame structure by using DenseNet trained from a simulated free vibration dataset. With limited measurement data, Zhang et al. [17] developed a one-dimensional CNN for the structural condition classification of a steel truss bridge and proposed the potential of GANs to generate reliable training data. Bao et al. [18] used a calibrated finite element model to pretrain a model for identifying various structural conditions and then applied transfer learning in the real testing domain. The aforementioned methods predict the parameters of actual structures by leveraging computational results from numerous numerical models under different states. They can effectively bridge the domain drifts between simulations and real measurements when the parameter range of the actual structure is determinable. However, the simulation using a large number of models with different initial parameters and even damage states requires a huge computational cost, especially for complex structures. Also, the sheer data volume can render the training of deep learning models challenging to be finished within a practical timeframe.

To circumvent the burdensome numerical simulations, another strategy that has attracted significant interest in recent years is to directly conduct domain adaptation on the structural responses. Domain adaptation (DA) is a special case of transfer learning, which focuses on reducing the discrepancies between different data distributions from source and target domains [19]. Gardner et al. [20] presented three DA techniques: Transfer Component Analysis, Joint Domain Adaptation and Adaptation Regularization-based Transfer Learning. They validated these methods through numerical simulations and a hybrid case study. In the latter, the source domain is composed of simulated data, while the target domain contains measurements from a three-floor frame structure. Recently, Gardner et al. [21] applied a domain-adopted Gaussian mixture model to align the frequency features of the data from the Z24 and KW351 bridges. Besides the above statistical approaches, more DA studies are there using deep CNNs. Wang and Xia [22] developed a re-weighted adversarial domain adaptation network by introducing a weight parameter in the DA process. The method was applied to two case studies, namely from one finite element (FE) model to others with different sizes and from a FE model to a small-scale cantilever beam. Chen et al. [23] combined 1D and 2D CNNs to extract features of vibration data and applied multi-kernel maximum mean discrepancy and local maximum mean discrepancy to align the data distributions between different measurement points of a steel grandstand. Martakis et al. [24] extracted damage-sensitive features of simulated and measured responses of a large-scale building model and deployed the Domain Adversarial Neural Network to transfer the knowledge obtained from simulations to real data for damage classification. The above-mentioned DA approaches were verified effective in reducing the difference between the data distributions of the source and target domains and improve the performance of the classifier trained on simulated data in the target domain. However, these methods predominantly serve as black boxes, outputting feature labels. Consequently, they fall short of directly producing structural responses post-DA, a critical component for the dynamic analysis of structures.

Generative adversarial learning makes it possible for DA to present the changes in structural responses [25,26]. Luleci and Catbas [27] applied the Domain-Generalized Cycle-Generative model to perform DA on the responses of two prestressed bridge FE models with different parameters under the same excitation of Gaussian noise. The results showed that the translated bridge state has similar frequencies and mode shapes to the target bridge. Following this study, Luleci et al. [28] modified the Cycle-Consistent Adversarial Networks (CycleGAN) into a DA model for 1D time series and then employed it to translate acceleration responses from undamaged to damaged states, gathered from a steel grandstand structure. As they found the ability of CycleGAN to reproduce frequency content was very limited, further improvements were reported in [29]. Gatti et al. [30] applied a Representation GAN to simulate and assess the transient dynamic responses of shear-type multi-story buildings under earthquake loading, enabling accurate damage classification and severity assessment by analyzing time-history data from multiple floors. The DA in these studies has achieved some success in the state translation among multiple FE models or varying states of a singular real structure. However, there is a very limited exploration of generative approaches to facilitate DA between simulated and actual structures, which can lead to more pronounced and unpredictable domain drifts. On the other hand, the fundamental component of the aforementioned GAN models remains the CNN. Numerous research has acknowledged CNNs for their excellent capability in local feature extraction, yet they fall short in handling long-range dependencies that are essential for time series in SHM applications [31,32]. While linear operations in fully connected layers, dense layers, or recurrent neural networks offer alternatives to capture long-range dependencies, these methods often require task-specific network architectures, resulting in less efficiency for processing signals across varying resolutions and dimensions.

Given the limitations identified in the above literature review, this research introduces an adapted CycleGAN. The proposed model uniquely integrates governing equations as physical constraints and incorporates the transformer for self-attention modules. The improvements not only offer better global feature extraction capability but also assure greater training stability compared to the original CycleGAN. More importantly, for the investigation of the DA among simulated and actual structural responses using the generative adversarial approach, this paper presents systematic experimental studies on both a steel beam and a large-scale steel truss bridge structure. The results show the superiority of the proposed DA model in both time and frequency domains.

The organization of the remainder of this paper is as follows. [Section 2](#) introduces the methodological framework. [Sections 3 and 4](#) discuss the experimental setups and their respective results. [Section 5](#) discusses the strengths and limitations of the proposed method, while [Section 6](#) presents the conclusion.

## 2. Methodology

### 2.1. GAN and CycleGAN

Generative Adversarial Networks (GANs), first introduced by Goodfellow et al. [33] in 2014, have been one of the most transformative ideas of deep learning. The essence of GANs lies in two neural networks: the generator (denoted as  $G$ ) and the discriminator (denoted as  $D$ ). They are used to generate samples with the input information and evaluate the generated samples, respectively. These two networks are typically trained in an alternating manner. The goal of the generator is to produce synthetic data that the discriminator cannot distinguish from real data, while the objective of the discriminator is to improve its ability to identify fake data. Such an iterative competition leads to the generator producing high-quality samples and can be mathematically expressed as,

$$\min_G \max_D \mathcal{L}_{adv} = \min_G \max_D \mathbb{E}_{y \sim p_{data}(y)} [\log D(y)] + \mathbb{E}_{x \sim p_{data}(x)} [\log (1 - D(G(x)))] \quad (1)$$

where  $\mathcal{L}_{adv}$  represents the adversarial loss,  $y$  the real data, and  $x$  the input information which is random noise in the initial GAN.  $\mathbb{E}_{y \sim p_{data}(y)}$  denotes the expectation computed over all the real data that follows the statistical distribution  $p_{data}(y)$ . The adversarial loss is the key idea behind GANs. Based on this concept, subsequent CNN-integrated models such as DCGAN [34], BigGAN [35], StyleGAN [36], etc. have consecutively emerged and achieved great success across numerous applications of computer vision, including image generation [37], image editing [38], representation learning [34], and image-to-image translation [39], i.e., the DA for images. However, in 2017, Zhu et al. [40] pointed out that traditional GANs necessitated paired datasets to learn the mapping between different domains. In reality, obtaining paired datasets is difficult and even impossible for some applications. To address this, they introduced the concept of cycle consistency and then proposed CycleGAN.

The CycleGAN is able to translate the datasets from two domains at the same time and with no requirement for data labels, thus, it is very suitable for SHM applications where the annotation of paired datasets is always costly. The DA approach proposed in this study is based on the fundamental idea of CycleGAN, and specially designed for the DA of acceleration signals. In the case that only CycleGAN is applied to the DA of acceleration signals, the DA process involves two mapping functions  $S(\cdot)$  and  $T(\cdot)$ , which are trained at the same time and respectively represent the mappings from the source and target domains. As shown in [Fig. 1](#),  $S(\cdot)$  and  $T(\cdot)$  are designed to be cycle-consistent and mathematically supposed to be inverses of each other, i.e.,  $\ddot{x}^c = T(S(\ddot{x})) \approx \ddot{x}$  and  $\ddot{y}^c = T(S(\ddot{y})) \approx \ddot{y}$ . The cycle-consistency loss measures the difference between the original acceleration  $\ddot{x}, \ddot{y}$  and the data  $\ddot{x}^c, \ddot{y}^c$  obtained after forward and inverse transformations, while the discriminators  $D_X$  and  $D_Y$  are used to determine the authenticity of the generated data  $\ddot{x}^c, \ddot{y}^c$ .

Different from GANs, the loss function of CycleGAN includes the adversarial loss  $\mathcal{L}_{adv}$ , cycle consistency loss  $\mathcal{L}_{cycle}$  and identity loss

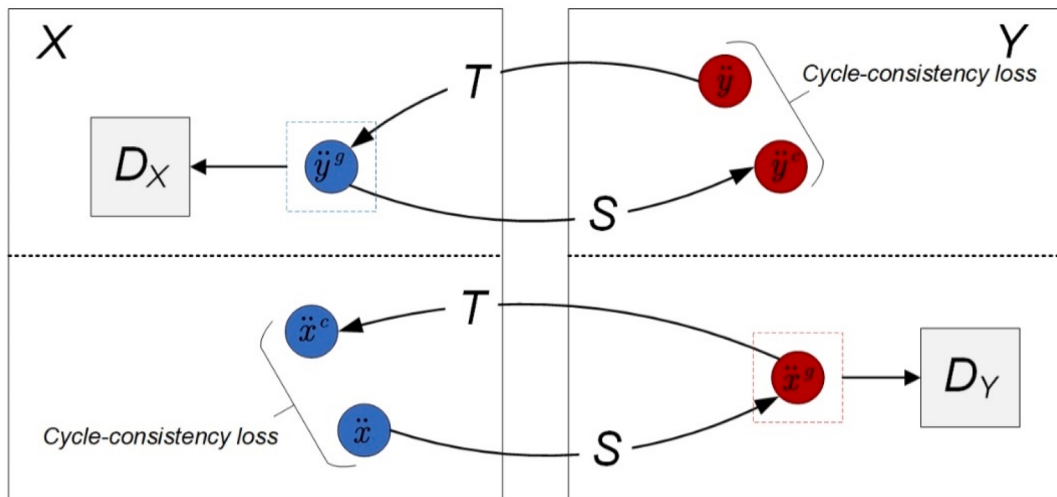


**Fig. 1.** Data transformation schematic between domains.

$\mathcal{L}_{idt}$ . For the mapping function  $S(\cdot) : X \mapsto Y$  and its corresponding discriminator  $D_Y$ ,  $\mathcal{L}_{adv}$  can be expressed as [40]:

$$\mathcal{L}_{adv}(S, D_Y, X, Y) = \lambda_{as} \mathbb{E}_{\ddot{x} \sim p_{data}(\ddot{x})} [(D_Y(S(\ddot{x})) - 1)^2] + \frac{\mathbb{E}_{\ddot{x} \sim p_{data}(\ddot{x})} [D_Y(S(\ddot{x}))^2] + \mathbb{E}_{\ddot{y} \sim p_{data}(\ddot{y})} [(D_Y(\ddot{y}) - 1)^2]}{2} \quad (2)$$

where  $\lambda_{as}$  represents the weight for the adversarial loss of the generator  $S$  and  $\mathbb{E}_{\ddot{x} \sim p_{data}(\ddot{x})}$  denotes the expectation computed over all acceleration data in domain  $X$  that follows the statistical distribution  $p_{data}(\ddot{x})$ . The first term on the right side of Eq. (1) is utilized for training the generator, while the second term is for training the discriminator.

The cycle consistency loss is for restricting the mapping functions to be cycle-consistent: as shown in Fig. 1, for each acceleration sequence  $\ddot{x}$  from domain  $X$ , the composite function of mapping functions  $S(\cdot)$  and  $T(\cdot)$  should map  $\ddot{x}$  back to a set of values that are approximately equal to the original values, i.e.,  $\ddot{x} \mapsto S(\ddot{x}) \mapsto T(S(\ddot{x})) \approx \ddot{x}$ . Similarly, the domain adaptation from domain  $Y$  to domain  $X$  should also be cycle-consistent. To this end,  $\mathcal{L}_{cycle}$  is given by:

$$\mathcal{L}_{cycle}(S, T) = \lambda_{cS} \mathbb{E}_{\ddot{x} \sim p_{data}(\ddot{x})} [\|T(S(\ddot{x})) - \ddot{x}\|_1] + \lambda_{cT} \mathbb{E}_{\ddot{y} \sim p_{data}(\ddot{y})} [\|S(T(\ddot{y})) - \ddot{y}\|_1] \quad (3)$$

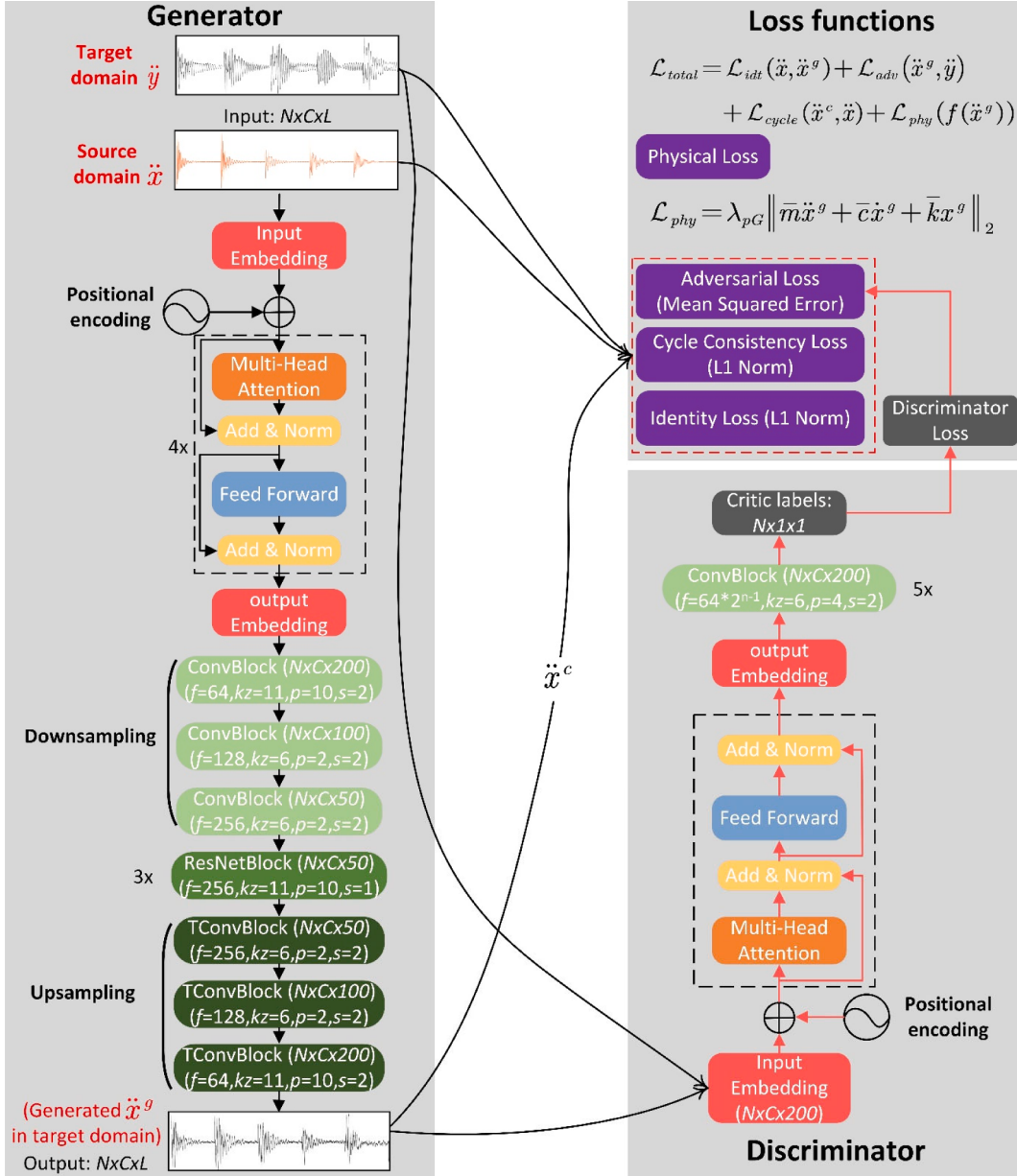


Fig. 2. Structure of the single network from domain  $X$  to domain  $Y$ .

where  $\lambda_{cS}$  and  $\lambda_{cT}$  represent the respective weights for the cycle consistency losses of mapping functions  $S$  and  $T$ .

The identity loss is designed to constrain the generator to retain the primary features of the input data while preventing unnecessary modifications. It is defined as:

$$\mathcal{L}_{idt}(S, T) = \lambda_{iS} \mathbb{E}_{\tilde{x} \sim p_{data}(\tilde{x})} [\|S(\tilde{x}) - \tilde{x}\|_1] + \lambda_{iT} \mathbb{E}_{\tilde{y} \sim p_{data}(\tilde{y})} [\|T(\tilde{y}) - \tilde{y}\|_1] \quad (4)$$

where  $\lambda_{iS}$  and  $\lambda_{iT}$  are weights for the identity losses of  $S$  and  $T$ . Then, the training objective of CycleGAN is to minimize the sum of the above three loss functions.

CycleGAN has achieved big success in the DA of images. However, when directly applied to long time series, it may struggle to effectively learn the global features of input data, potentially leading to unstable training [31,32]. Thus, the study [29] incorporated Gated Linear Units, which include linear transformations to improve their CycleGAN-based model presented in [20]. Targeting time series in varying dimensions, the objective of this paper is to develop an improved CycleGAN model for more robust DA for time series in SHM.

## 2.2. The proposed DA model

This subsection introduces two improvements for the original CycleGAN: one concerning the network architecture and the other related to the loss function. Since the proposed DA model has two symmetrical networks used for training the mapping functions  $S(\cdot)$  and  $T(\cdot)$ , only the single network for the transformation from domain  $X$  to domain  $Y$  is illustrated for simplicity. Fig. 2 presents the network structure and the forward data propagation process during the training phase. The input to the generator is a  $N \times C \times L$  tensor from domain  $X$ , where  $N$  stands for the batch size,  $C$  for the number of channels, and  $L$  represents the length of the time series. The generator outputs a tensor of the same dimensions as the input, which is anticipated to align with the feature distribution of domain  $Y$ .

In contrast to CycleGAN, the proposed model integrates an additional transformer encoder in the preliminary layers of both the generator and discriminator, enhancing the ability to learn global features. The transformer, originally introduced by Vaswani et al. [41], is noted for handling long-range dependencies in data without any significant loss in performance due to its self-attention mechanism, while CNNs tend to rely on local receptive fields. Another advantage of the transformer is its flexibility regarding the length of the input time series. In this study, all the time series with a length of  $L$  are uniformly encoded into feature vectors of length 200, which are noted as input embedding in Fig. 2. To make use of the order of the time series and learn temporal dependencies, position encodings are separately assigned to each element of the input embedding using sine and cosine functions [41]. Then, in the multi-head attention module, four heads are employed to strike a balance between model complexity and performance. Following this, after the operations of residual connections, addition and layer normalization with a dropout rate of 0.1, the transformer encoder produces an output embedding with the same size. The output embedding then goes through convolutional blocks (ConvBlock), residual network blocks (ResNetBlock) and deconvolutional blocks (TConvBlock). While these operations are derived from CycleGAN, the original activation function ReLU is replaced by LeakyReLU [42] in the proposed model. The number of filters, convolution kernel size, padding and stride are denoted as  $f$ ,  $kz$ ,  $p$  and  $s$ , respectively, in Fig. 2. The values of  $f$  and  $s$  in the original CycleGAN [40] are employed here, while  $kz$  and  $p$  are determined through multiple experiments to get a trade-off between model performance and complexity.

Besides the self-attention modules, the inclusion of a physical loss, which is denoted as  $\mathcal{L}_{phy}$ , is the second highlight of the proposed DA model. It is known that for linear structural systems, the structural response can be obtained by modal superposition. The responses of the  $i^{th}$  mode  $r_i(t)$  can be described by the governing equation,

$$m_i \ddot{r}_i(t) + c_i \dot{r}_i(t) + k_i r_i(t) = p_i(t) \quad (5)$$

where  $m_i$ ,  $c_i$  and  $k_i$  represent the modal mass, modal damping and modal stiffness, respectively, while  $p_i$  denotes the generalized force. In most cases, the structural responses can be represented by the linear superposition of a few dominant modes. To describe the combined effect of the dominant modes, it is assumed that there exists an equivalent mode that satisfies

$$\bar{m} \ddot{r}(t) + \bar{c} \dot{r}(t) + \bar{k} r(t) = p(t) + \epsilon(t) \quad (6)$$

In this equation,  $\bar{m}$ ,  $\bar{c}$  and  $\bar{k}$  are equivalent parameters that are trainable in the DA model.  $r(t)$  and  $p(t)$  are the sums of the responses and generalized force of  $n$  dominant modes, i.e.,  $r(t) = \sum_{i=1}^n r_i(t)$  and  $p(t) = \sum_{i=1}^n p_i(t)$ .  $\epsilon(t)$  denotes the residual term caused by noise and numerical errors and can be physically regarded as a virtual time-varying force. The physical loss is to minimize the energy of  $\epsilon(t)$ . For the free vibration, the  $p(t)$  becomes zero. Then, by replacing  $r(t)$  in Equation (6) with  $x$ ,  $\mathcal{L}_{phy}$  is defined as

$$\mathcal{L}_{phy}(S, T) = \lambda_{ps} \mathbb{E}_{\tilde{x} \sim p_{data}(\tilde{x})} [\|\bar{m}_S \ddot{x}^g + \bar{c}_S \dot{x}^g + \bar{k}_S x^g\|_2] + \lambda_{pt} \mathbb{E}_{\tilde{y} \sim p_{data}(\tilde{y})} [\|\bar{m}_T \ddot{y}^g + \bar{c}_T \dot{y}^g + \bar{k}_T y^g\|_2] \quad (7)$$

where  $\lambda_{ps}$  and  $\lambda_{pt}$  are weights respectively for the generator  $S$  and  $T$ . It should be noted that the displacement and velocity data in Eq. (7) can generally be obtained through the integration of acceleration. The physical loss guides the generated signals towards the average effect of several dominant modes, thereby avoiding random divergence of the signal and enhancing the physical interpretability of the output results. Then, the total loss can be obtained by

$$\mathcal{L}_{total} = \mathcal{L}_{adv}(S, D_Y, X, Y) + \mathcal{L}_{adv}(T, D_X, Y, X) + \mathcal{L}_{cycle}(S, T) + \mathcal{L}_{idt}(S, T) + \mathcal{L}_{phy}(S, T) \quad (8)$$

### 2.3. Training strategy

Incorporating the self-attention mechanism and physical constraints is beneficial for improving the performance and training robustness of the generator. Apart from the improvements in the network architecture, some training strategies are also applied in this study. Firstly, synchronized data from multiple measurement points are employed during the training phase to preserve the intrinsic modal characteristics after post-domain adaptation. The training data is processed via filtering in advance, which helps to remove high-frequency and low-energy components and minimize errors induced by acceleration integration within the physical loss. Secondly, to combat the risk of overfitting, the AdamW [43] optimizer is adopted, superseding the conventional Adam algorithm from the original CycleGAN, accompanied by a more conservative learning rate. Lastly, acknowledging the potential disparity in training velocities between the generator and discriminator, their parameter update rates are carefully optimized according to the specificities of training datasets. Detailed information regarding the training parameters and weights adopted in this study is elucidated in [Sections 3 and 4](#).

### 2.4. Evaluation methods

In the studies of image domain adaptation, qualitative comparison for the generated and original images is an intuitive way of model evaluation, but its intuitiveness diminishes greatly for time series data. Therefore, this study conducts a quantitative comparison to assess the performance of the proposed DA model from three distinct perspectives: time domain, frequency domain and mode shapes.

In the time domain, Mean Square Error (MSE) is used to measure the similarity between the generated acceleration and the actual acceleration in the target domain, because MSE can effectively reflect local discrepancies by calculating the squared difference. For the comparison in the frequency domain, the fast Fourier transform is applied to both the generated and actual acceleration. The Magnitude Squared Coherence (MSC) is employed to present the similarity of frequency spectrums, and the averaged MSC over all the samples is defined as Mean Magnitude Squared Coherence (MMSC), which is expressed as [20],

$$\text{MMSC} = \frac{1}{N} \sum_{i=1}^N \frac{|S_{i,xg}|^2}{S_{i,xx} \times S_{i,gg}} \quad (9)$$

where  $S_{i,xg}$  is the cross-spectral density estimate, while  $S_{i,xx}$  and  $S_{i,gg}$  are the power spectral density estimates of the measured and generated datasets. When the generated data is similar to the actual one, MMSC gets close to 1, otherwise to 0. For the SHM applications, the reproduction quality of mode shapes is important for the proposed DA model. In this study, modal identification is conducted on the generated and real acceleration and the modal assurance criterion (MAC) is used to assess the similarity of identified mode shapes.

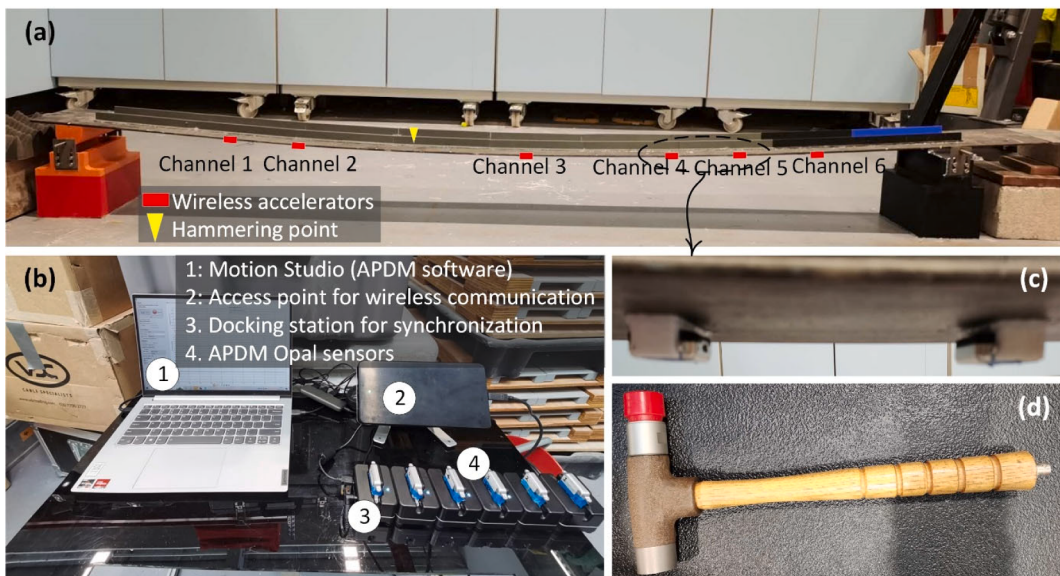


**Fig. 3.** Experiment setup for the free vibration tests: (a) steel beam; (b) APDM system; (c) installed sensors; (d) test hammer.

### 3. Experimental validation on steel beam model

Free-vibration responses are garnering increasing attention in SHM due to their high signal-to-noise ratio and superior discernibility of modal characteristics [44,45]. To demonstrate the DA capability of the proposed approach, a series of free-vibration tests were conducted on an experimental beam and are detailed in this section.

#### 3.1. Laboratory experiments for target domain dataset

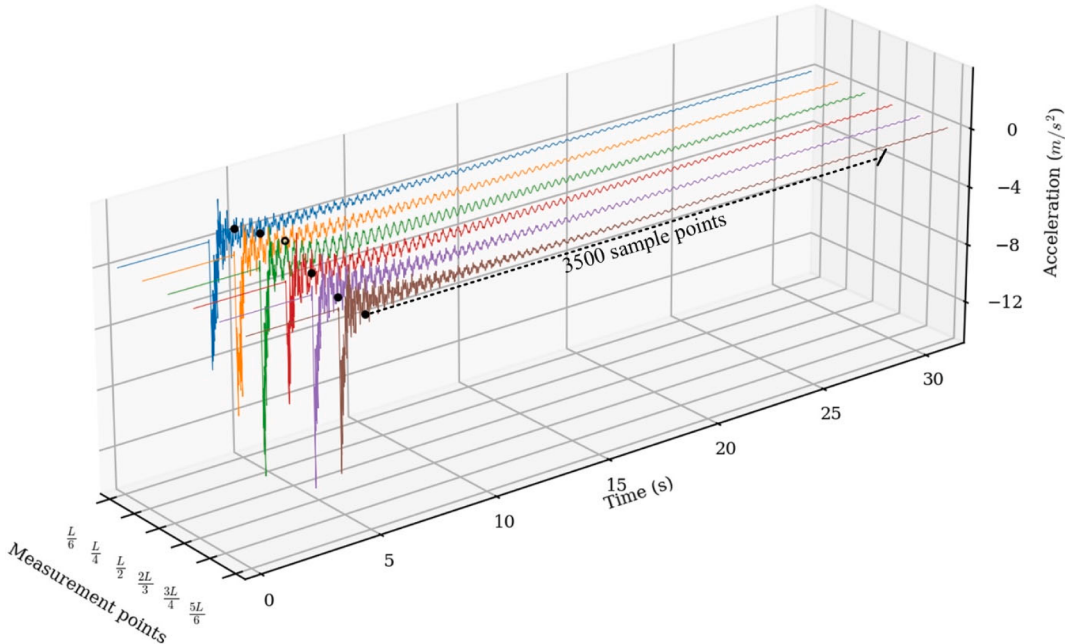
A simply supported beam with cantilevers at ends is selected for free-vibration tests. As shown in Fig. 3, the test structure is a steel beam with dimensions of  $2.49\text{m} \times 20\text{cm} \times 6\text{mm}$  and a  $2.16\text{ m}$  distance between the supports. Six Opal wireless sensors were used for acceleration measurements. They were installed beneath the beam at positions of  $1/6$ ,  $1/4$ ,  $1/2$ ,  $2/3$ ,  $3/4$  and  $5/6$  spans, respectively, as shown in Fig. 3(a) and (c) and were synchronized with a docking station before installation. The data streams from different sensors were transferred to the access point wirelessly and then recorded by the Motion Studio, a software suite bundled with the APDM monitoring system, as shown in Fig. 3(b). The impact force was acted at around  $5/12$  span using a test hammer shown in Fig. 3(d). A total of 100 repeated free vibration tests were carried out to obtain attenuation responses under different impact forces. The sampling frequency of accelerators was set as 128 Hz while the measurement range of  $-2 \sim 2\text{ g}$ .

Fig. 4 shows the vertical acceleration of six measurement points subjected to an impact force. It can be observed that the signals from different channels were well synchronized, and obvious negative peaks caused by hammering can be observed. After the first negative peaks, the signals exhibit typical patterns of free decaying. Given this, to eliminate the response segment during the contact period between the test hammer and the structure, the response at the mid-span (i.e., green curve) was taken as the reference. The signal was truncated starting from the third peak, and the length of the signal was uniformly set to 3500 sample points, as shown in Fig. 4. It is seen that the signals of different channels are not simultaneously at the peak at the start points of truncated samples, indicating a regular phase difference in various positions along the test beam.

During the 100 repeated hammering tests, the magnitude of the applied force was intentionally left uncontrolled to reproduce the unknown initial amplitude of attenuation responses in real-world structures. However, for model training, it is still necessary to standardize the input responses to mitigate any adverse effects resulting from varying scales. Once again, Channel 3 was selected as the reference. The responses in Channel 3 from different tests were first individually normalized by dividing their maximum values, and then the responses of other channels were scaled by the same proportion. In this way, a dataset for the target domain was obtained, containing 100 sets of normalized time series from 6 channels in size of  $3500 \times 1$ .

#### 3.2. Numerical simulations for source domain dataset

Real-world structures are generally regarded as homogeneous with their numerical simulation models (e.g. FE models), in terms of geometry, materials and topology. The difference in data distributions between actual and simulated structures comes from



**Fig. 4.** Free-vibration responses measured from the steel beam.

assumptions of material properties, boundary conditions and load patterns, etc. For the test beam discussed in this section, the cantilever at both ends was neglected in FE modelling and thus simplified to a standard simply supported beam. As shown in Fig. 5, the model was composed of 12 constant-sectional beam elements. The impulse force was used for simulating hammer loads. Six nodes were selected to calculate decaying responses responding to signals collected by the six sensors in laboratory experiments.

The FE model was realized with the structural parameters listed in Table 1. The structural damping was modelled as Rayleigh damping, while the damping ratio  $\xi$  was assumed at the same value of 0.02 for the first three modes [46]. To calculate acceleration responses, Newmark  $\beta$  method was applied with a 1/128 s calculation time interval, corresponding to the sampling frequency of accelerometers. Same as the laboratory experiments, the numerical simulation was also repeated by 100 times, and the impulse force in each repetition was set as the same value as the peak accelerations measured in Channel 3, i.e., the circle in Fig. 4. In addition, considering the observation errors, three different levels of 1 %, 5 % and 10 % white noise were respectively added into the calculated responses of six channels, followed by data normalization, and then yielding a simulated dataset in the source domain with the same size as the measurements in the target domain.

### 3.3. Training of the proposed DA model

The samples obtained through experiments and FE simulation were both used in the training of DA models. As introduced in Section 2, the proposed model can realize the mutual transformation between the measurement and simulation domains through a single training, benefiting from the idea of cycle consistency. This section presents the training process and illustrates the superiority of the proposed model compared to the original CycleGAN.

To initially evaluate the correctness of the FE model and the distribution of simulated data, frequency analysis for structural responses in both domains was conducted. Table 2 presents the first three vertical bending frequencies of the test beam and the FE model with different bending stiffnesses. The frequencies of the test beam and the FE model are shown close, indicating the modelling is reliable. However, the DA for such small differences is relatively easy and not ideal for demonstrating the performance of DA models. Therefore, to increase the domain drifts, this section uses the FE model with 80 % stiffness reduction for the training and testing of DA models.

The measured and simulated datasets were divided into training and test sets in a 9:1 ratio, and the size of each sample was  $6 \times 3500$ , representing the number of channels and data length, respectively. The parameters in Table 3 were used for the model training.

To assess the performance of DA models, the MMSC score, Adversarial Loss and MSE were utilized to monitor the training process. In addition, to distinguish the advantages of the proposed model from the original CycleGAN, three different models were compared, including the proposed model (Model A), the proposed model without physical loss (Model B) and the original CycleGAN (Model C). The hyperparameters for the same parts of these three models remained consistent. All the models were trained for 250 epochs on the same computer equipped with an Nvidia RTX A6000 GPU. It is found through experiments that DA from the simulation domain to the measurement domain is more difficult than that in the opposite direction. In this regard, the following discussion only focuses on the training from simulations to measurements for brevity.

With the real and synthetic accelerations, trends in metrics such as MMSC scores, Adversarial Loss and MSE were calculated during the training of Model A, B and C, of which the results are presented in Fig. 6. Several interesting observations can be made from the sub-figures:

- (1) When comparing models A and C, it is evident that the proposed self-attention-enhanced model yielded higher MMSC scores in the frequency domain.
- (2) Fig. 6(b) reveals that the Adversarial Loss of Model C exhibited fluctuations even after falling to a certain range, while those of Models A and B, with self-attention modules, displayed smoother patterns, indicating better training stability.
- (3) In comparison to Model B, which has no physical loss, the Adversarial Loss and MSE of Model A presented smaller oscillations, suggesting using governing equations as physical constraints to guide model training can further improve the stability of convergence.

The above experiment reveals the superiority of integrating self-attention mechanisms with CNNs in terms of model performance. It also reflects the positive guiding role of physical information in generative models. These findings not only validate the proposed approach but also provide valuable insights for developing novel DA models in SHM.

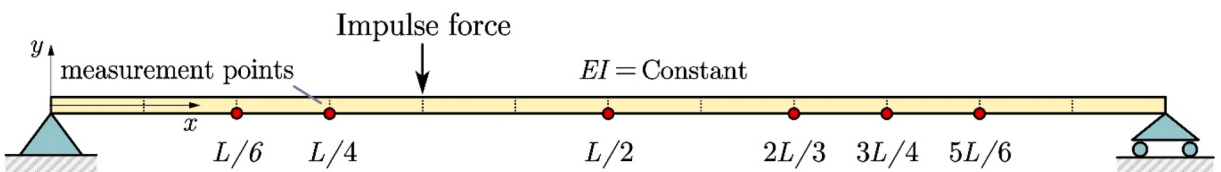


**Fig. 5.** Finite element model of the simply supported beam.

**Table 1**

Modelling parameters of the simply-supported beam.

Parameters	$L$	$EI$	$A$	$\rho$	$\xi$
Values	2.16 m	756 N · m <sup>2</sup>	0.0012 m <sup>2</sup>	7800 kg/m <sup>3</sup>	0.02

**Table 2**

Modal frequencies of the test beam and FE models.

Model (Stiffness)	$\omega_1$	$\omega_2$	$\omega_3$
FE model (EI)	3.07 Hz	11.81 Hz	24.03 Hz
Test beam (unknown)	3.09 Hz	10.77 Hz	26.42 Hz
FE model (20 % EI)	1.37 Hz	5.39 Hz	11.90 Hz

**Table 3**

Hyperparameters for the training of the DA models.

$\lambda_{as}$	20
$\lambda_{aT}, \lambda_{cS}, \lambda_{cT}, \lambda_{pS}, \lambda_{pT}$	10
$\lambda_{IS}, \lambda_{IT}$	0
Discriminator updating frequency	1 time per 5 epochs
Learning rate for Generators	0.0001
Learning rate for Discriminators	0.0001
Batch size	5

### 3.4. Testing and assessment for the trained DA model

A 10 % subset of the dataset was used for model testing. In contrast to the training process, model testing involves utilizing single-domain data as input to generate synthetic samples while using the other domain data to assess the synthetic outputs. As discussed in Section 3.3, the DA from measurement to simulation tends to yield favorable results, given the relatively easier distributions in the simulation domain. Hence, to provide more robust validation, this section focuses on the testing of the trained DA model for the DA process from simulation to measurement, considering varying levels of noise.

Fig. 7 shows clips of the mid-span (Channel 3) acceleration responses before and after DA. It can be seen in Fig. 7(a) that the simulated acceleration (with 5 % additional noise and 80 % stiffness reduction) is significantly different from the measurement. However, when applying the trained DA model to the simulated data, a synthetic response, which is shown in good agreement with the measured one, can be obtained, as shown in Fig. 7(b). Correspondingly, the value of the metric MSE was greatly reduced.

Besides the comparison in the time domain, Fig. 8 presents the Fourier spectrums of the acceleration responses from Channel 3. It is shown that the proposed DA model successfully generates synthetic responses, which have similar frequencies as the actual measurements, by using the simulated responses with different levels of white noise. Accordingly, the MMSC scores were significantly increased. However, it is still noticeable that there are errors in the peak values of the frequencies, which may affect the accuracy of mode shapes.

For further investigation, modal identification was conducted on both the measured and synthetic responses using SSI-Cov algorithm [47]. Fig. 9 gives the identified mode shapes for 5 % noise. It can be seen that the first two mode shapes identified from the generated responses are in good agreement with those from the measured ones. The third mode is possibly a torsional mode and cannot be reflected in the beam-like FE model, but it was still successfully reconstructed, suggesting the proposed model well learned the data characteristics of the measurement domain. The fourth mode has the smallest energy and is almost indistinguishable in Fig. 8, resulting in more differences in the identification results of the mode shapes. To quantify the differences, the modal assurance criterion (MAC) was calculated for all modes and noise cases, of which the results are listed in Table 4. It is evident that using ten sets of synthetic samples can effectively identify the first three modes while maintaining a high degree of similarity with the measured mode shapes. However, the recognition rate (the rate of correctly identifying the mode shapes) and MAC for the fourth mode shape experienced a slight decrease. It is worth noting that noise has less influence on low-order modes with high energy proportion but more significant influence on high-order modes. Therefore, it is recommended to focus only on the few dominant modes in practical applications.

## 4. Experimental validation on a steel truss bridge

In order to demonstrate the performance of the proposed DA model on complex structures, this section presents details of an experiment conducted on a large-scale bridge model.

### 4.1. Experimental setup

The test structure is a steel truss bridge measuring 7.06m × 1.11m × 1.47m, composed of 70 members connected by bolts. Similar to

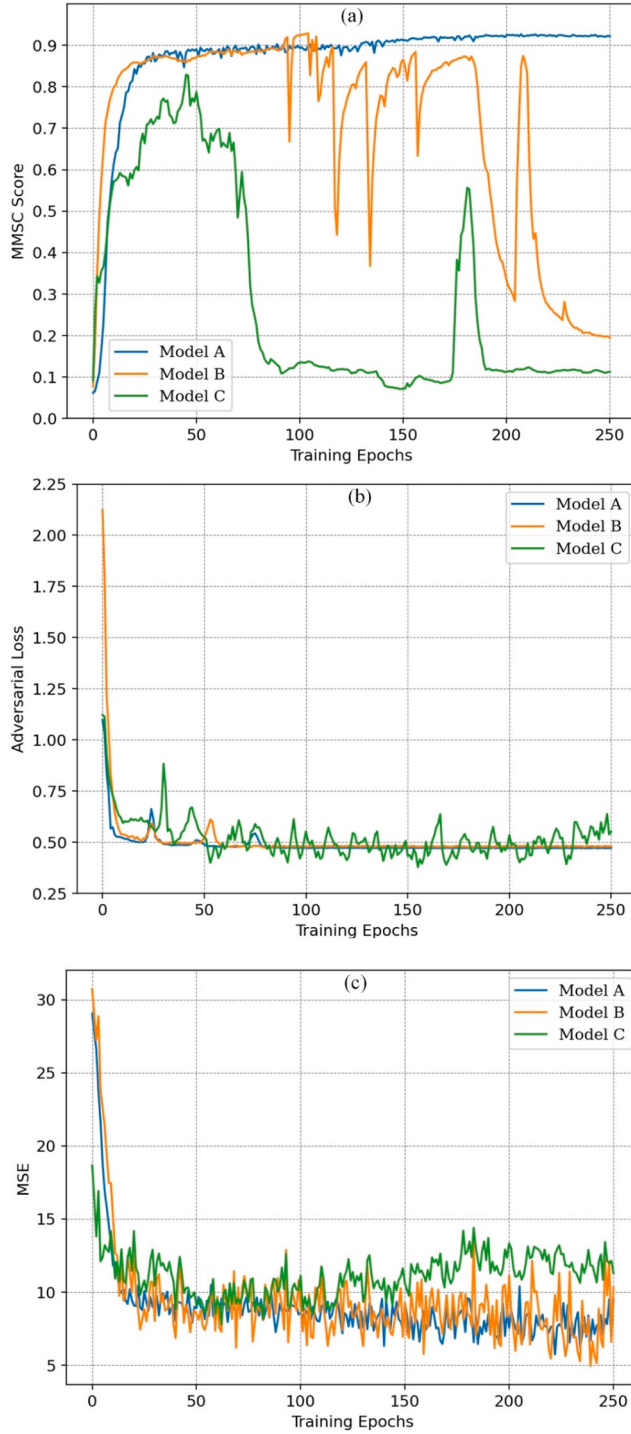


**Fig. 6.** Comparison of the training process for different DA models (5% noise): (a) MMSC score; (b) Adversarial Loss; (c) MSE.

the experiments in [Section 3](#), the free decay acceleration from the simulation and measurement was used for DA. As shown in [Fig. 10](#), the FE model of the experimental structure was created with SAP2000. All members were modelled according to the actual cross-sections using linear frame elements. Bolted connections were simplified to be rigid, and the damping ratio for modal analysis was set to 0.02. To induce vertical vibration, impulse forces with different peak values were employed in the FE model, while a rubber hammer was used to strike the same position on the test bridge, as denoted by the red arrows in [Fig. 10](#). Six PCB accelerometers were installed at locations of 1/8, 1/4, 3/8, 1/2, 5/8 and 3/4 span along the central axis, sampling at a frequency of 512 Hz. The six

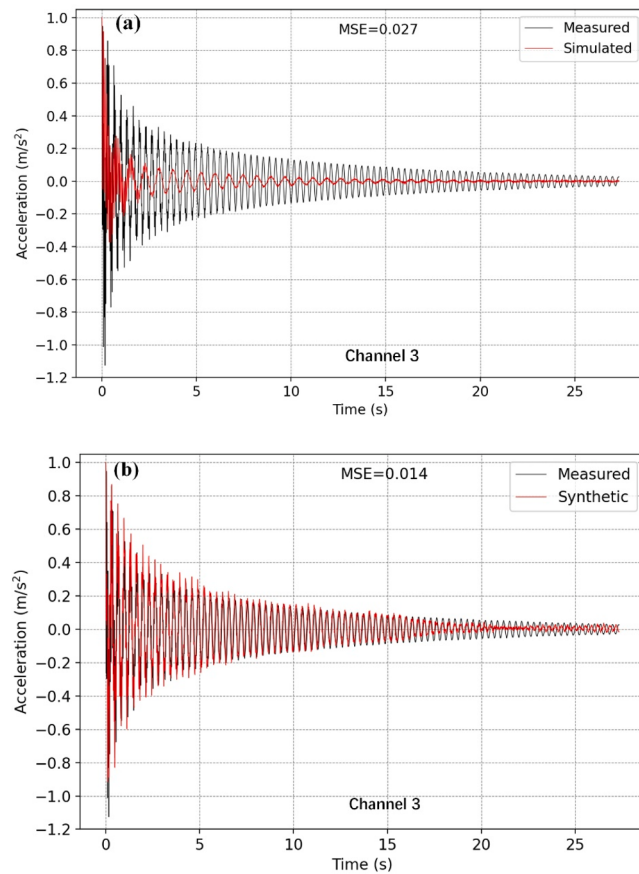


**Fig. 7.** Comparison of the acceleration responses: (a) before DA; (b) after DA.

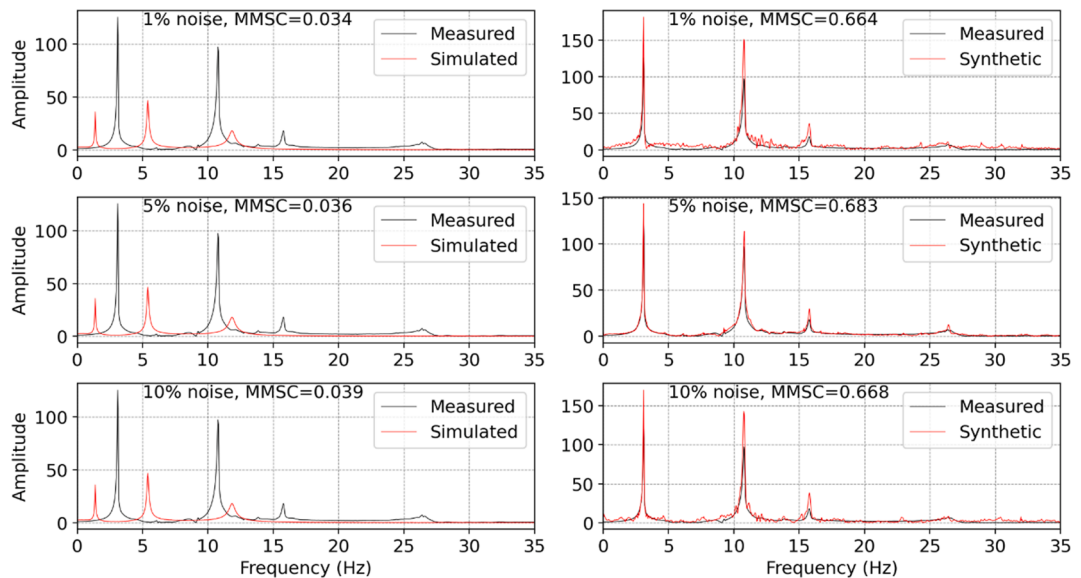


**Fig. 8.** Frequency domain comparison of Channel 3 responses for different levels of noise.

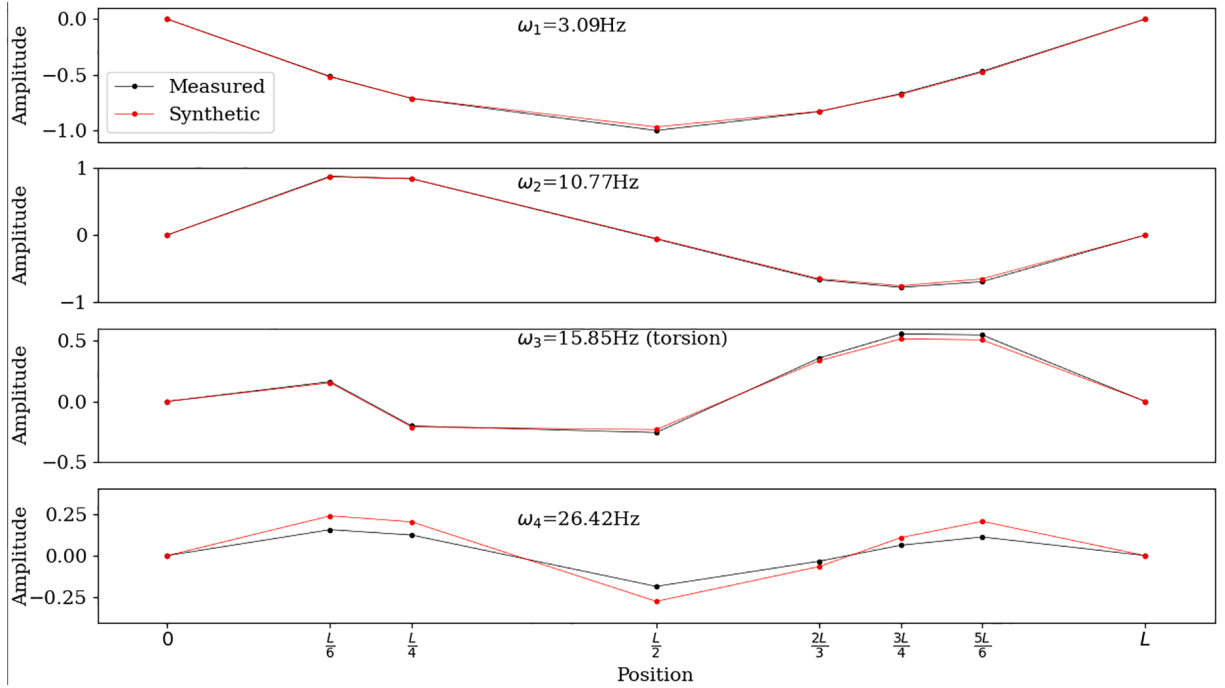


**Fig. 9.** Comparison of the mode shapes identified from measured and synthetic responses.

**Table 4**

Averaged MAC values between the measured and synthetic mode shapes.

Noise level	1st mode	2nd mode	3rd mode(torsion)	4th mode
1 %	0.9997	0.9992	0.9912	0.9539
5 %	0.9997	0.9995	0.9992	0.9899
10 %	0.9994	0.9996	0.9804	0.9089
Recognition rate	100 %	100 %	100 %	90 %

measurement channels are labelled as C1-6, as shown in Fig. 10(b).

In this experiment, the hammering test was repeated 110 times without artificially controlling the hammering force. To keep consistent with actual tests, the impulse forces in the simulation were determined by the maximum acceleration at the mid-span (channel 4), and 5 % noise was added to simulated responses to mimic observation errors. Then, all the simulated and measured responses were standardized based on the peak acceleration in channel 4 using the same method described in Section 3 and were further truncated into samples in a uniform length of 2500, as shown in Fig. 11. A total of 110 sets of measured and simulated acceleration samples were collected across all channels and then partitioned into training and test sets according to the ratio of 9:1 to verify the proposed DA model.

#### 4.2. Training configuration

In contrast to the steel beam tested in Section 3, the steel truss bridge exhibits higher damping, resulting in faster vibration attenuation. Therefore, the sample length was reduced from 3500 to 2500. Notably, the self-attention module in the proposed model is adaptable to input samples of varying lengths, so there is no need for the modification of the model architecture. However, the steel bridge has a high level of structural complexity, and significant diversity exists in the responses obtained from repeated measurements, which pose challenges for the learning of signal features. To reduce the difficulty of feature learning and ensure training stability, two adjustments were made in this section. Firstly, low-pass filtering was applied to the datasets to disregard high-frequency components above 35 Hz. Secondly, identity loss was considered in this case to preserve the essential characteristics of the signals of the source domain, thus preventing the generator from producing meaningless outputs. The proposed model was trained for 250 epochs with the same parameters as in Table 3, except that the weight of identity loss was set to 10. A direct evaluation of the domain adaptation results is presented below.

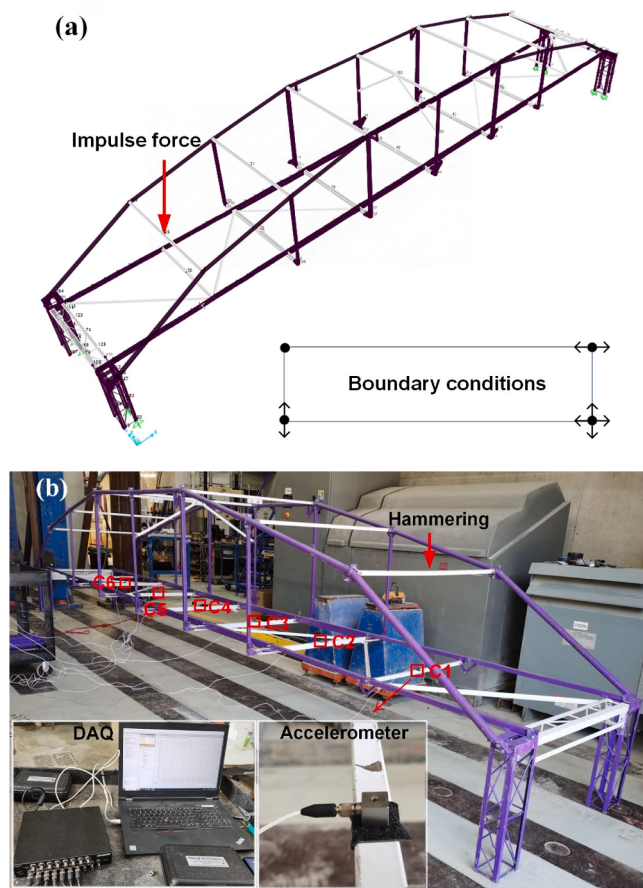


**Fig. 10.** Steel truss bridge: (a) FE model; (b) laboratory test structure.

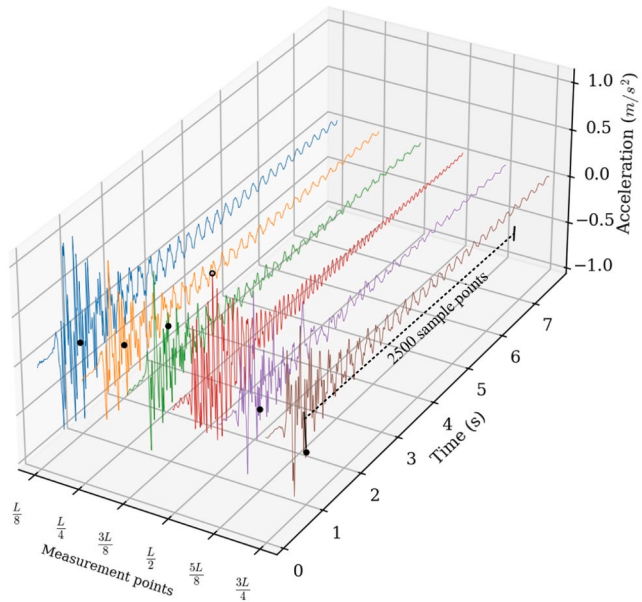


**Fig. 11.** Free-vibration responses measured from the steel bridge.

#### 4.3. Testing results

The trained DA model was applied to the test set for the DA from simulated to measured acceleration. Similarly, the acceleration signals generated from simulated samples were again evaluated with the similarity in the time domain, frequency domain and mode shapes. Firstly, the average value of MSEs between the synthetic and measured acceleration was calculated in the time domain. It was shown that the mean MSE decreased from 0.21 to 0.15, indicating an increase in similarity. Then, as shown in Fig. 12, the signals of three selected channels were compared after Fourier transform. It is evident that before DA, both the measured and simulated signals exhibit four prominent frequencies, but their spectral distributions differ significantly. However, after applying the proposed DA model, the first two frequencies were successfully reconstructed in the synthetic signals, while the higher-order frequencies were not as accurately reproduced due to their lower magnitudes. Moreover, the metric MMSC scores, which are positively correlated with similarity, presented a significant increase after DA.

Finally, the SSI-Cov algorithm [47] was applied to both the measured and synthetic signals, with the MAC values serving as the basis for determining the similarity of the identified modes. It was observed that the modal information obtained from different repeated tests was not entirely consistent. This inconsistency may be attributed to the complex friction effects that exist between the bridge components. Therefore, to increase the sample length and enhance the accuracy of identification results, the 11 test samples were concatenated before modal identification. To ensure the objectivity of the comparison, the parameters in the SSI-Cov algorithm were set identically for both signals.

Fig. 13 shows the four mode shapes identified from both signal groups, corresponding to the first four frequencies of the measured signals at 4.11 Hz, 8.97 Hz, 18.45 Hz, and 25.17 Hz. It is shown that the modal information of the synthetic signals aligns closely with that of the measurements, particularly at lower orders. As the frequency increases, the MAC values demonstrate a decreasing trend. In addition, it is noted that the first mode obtained in this experiment did not present the shape of the first-order vertical bending, but rather resembled a second-order vertical bending. To further investigate this phenomenon, the FE model was employed for modal analysis to explore the intrinsic characteristics of the bridge itself. The analysis results also showed the first-order vertical bending mode was inactive. In an effort to explore the reasons, modes manifesting overall vertical bending with frequencies below 35 Hz were carefully selected, and their modal participation factors are listed in Table 5. In the table, X, Y, and Z denote the along-bridge, cross-bridge, and vertical directions, respectively, while  $R_x$ ,  $R_y$ , and  $R_z$  correspond to the rotations around these axes. The modal participation factor, a dimensionless number, indicates the contribution of a specific mode to a particular degree of freedom.

Several noteworthy observations can be found in Table 5. Firstly, the along-bridge vibration played a dominant role in the mode corresponding to 3.73 Hz, suggesting that the mode shape resembling the second-order vertical bending, as depicted in Fig. 13(a), was possibly caused by along-bridge vibration. This occurrence could be attributed to the central part of the bridge having significantly greater stiffness than the sides and the legs having relatively low stiffness in contrast to the main beam. Additionally, the mode near 25.92 Hz exhibited a fourth-order vertical bending shape, but it is revealed from Table 5 that the vertical vibration did not make a significant contribution. The observed vertical component could possibly stem from the along-bridge vibration or lateral torsion. Overall, the modal characteristics of the steel bridge were complex and might be influenced by the experimental settings and modal identification algorithms. However, the acceleration responses generated from the simulation were shown in good agreement with the measured ones, demonstrating that the proposed approach possesses the robust capability of DA.

## 5. Discussions

The generative DA model proposed in this paper successfully achieved the mutual transformation of simulated and measured structural responses for both a steel beam and a large-scale truss bridge, underscoring promising potential in mitigating domain drifts. However, it remains necessary to discuss its limitations and areas deserving of subsequent research. It should be noted that the free-vibration responses adopted in this paper can be induced in actual bridges by the passage of vehicles [13,45]. However, for cases where the vehicular load is negligible compared to the self-weight of the bridge, such as in long-span bridges, responses to ambient excitation can be more pragmatic.

Although this study primarily addresses free-vibration scenarios, it is necessary to highlight that with an ample number of training samples induced by ambient excitation, the value of  $p(t)$  in Equation (5) can converge to zero post-normalization, owing to the property that any linear combination of Gaussian-distributed components remains Gaussian-distributed. This suggests that the proposed DA model is theoretically applicable to cases under ambient excitation. The physical loss introduced in this paper formally guides the generator to retain the most critical modal information. It is possible to further improve the DA results by employing multimodal physical constraints and multiple generators. In addition, although the proposed method combines the strengths of self-attention and CNNs, the hyperparameters presented are merely one feasible set, and further optimization tailored to specific datasets remains possible.

## 6. Conclusions

In this paper, a novel generative DA model that integrates the self-attention mechanism and physical constraints of the linear dynamic system is proposed to achieve DA between the FE models and real engineering structures. The DA approach is verified effective through free-vibration tests on two scales of bridge models. Based on the experimental results, some conclusions can be obtained.

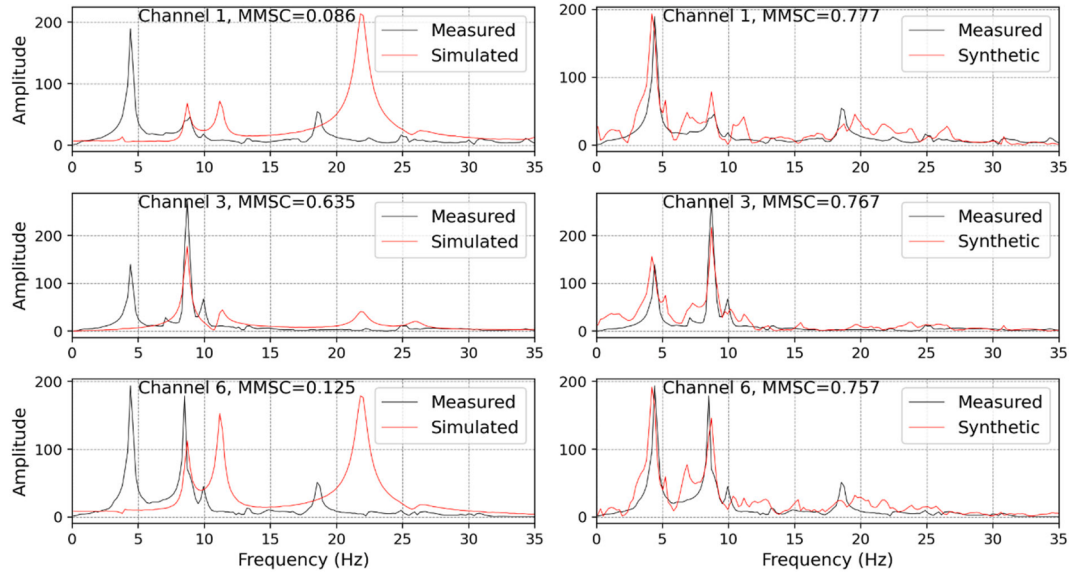


Fig. 12. Frequency domain comparison for different channels.

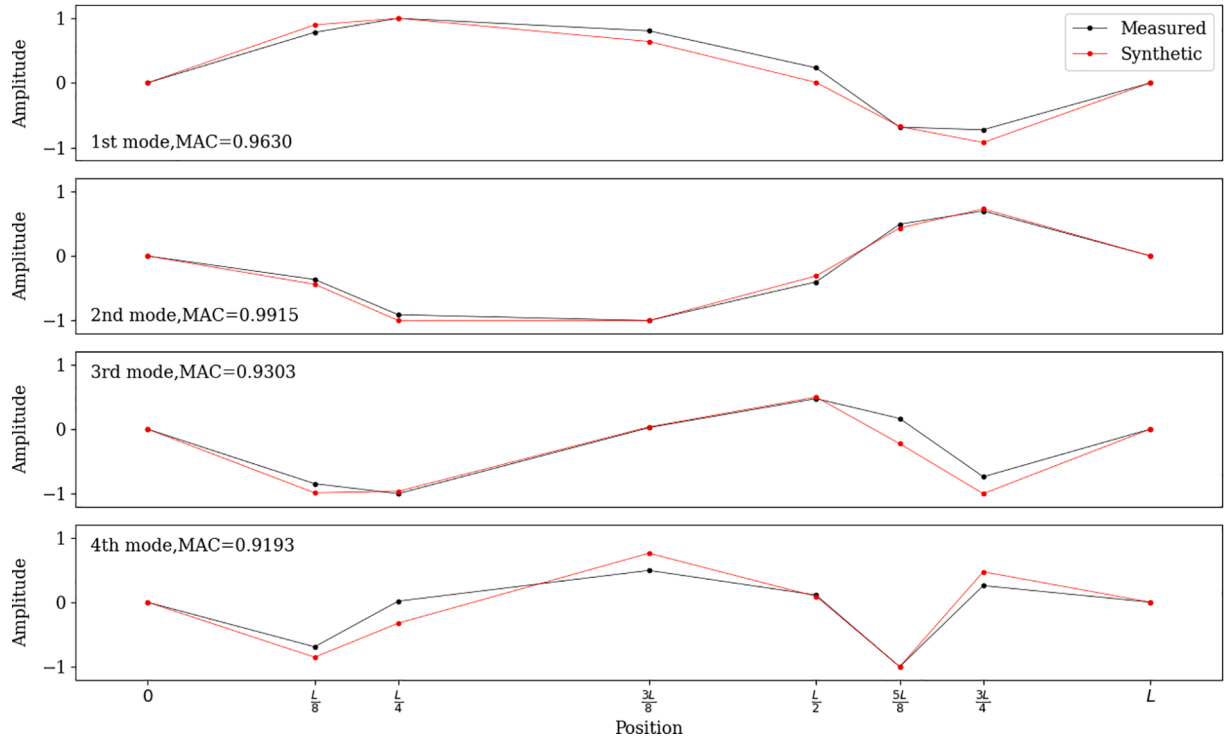


Fig. 13. Mode shapes identified through measured and synthetic acceleration.

1. Through comparative experiments on a steel beam model, it was demonstrated that the self-attention modules can significantly enhance the performance of the CNN-based generative DA model. Both the self-attention module and physical constraints contribute to improving the stability of GAN training.
2. The experimental structures used in this study exhibit substantial discrepancies in structural parameters compared to their FE models. Nonetheless, the proposed DA model successfully learned the mapping relationships between the simulation and measurement domains and delivered good performance on previously unseen test data.

**Table 5**

Modal participating mass ratios of identified modes.

Frequencies	X (%)	Y (%)	Z (%)	R <sub>X</sub> (%)	R <sub>Y</sub> (%)	R <sub>Z</sub> (%)
3.73	86	<0.01	0.49	<0.01	2.05	<0.01
8.57	3.70	<0.01	15	<0.01	12	<0.01
21.81	<0.01	0.05	22	0.06	0.04	<0.01
25.92	0.72	<0.01	0.02	0.31	<0.01	<0.01

3. The proposed method exhibits superior performance in the DA of low-order modal responses compared to higher-order models. Additionally, it demonstrates reduced sensitivity to noise interference.

The proposed DA approach is demonstrated on the structures in unchanged structural states. For future endeavors, it is recommended to conduct DA research among multiple structural states to serve model updating and damage detection in SHM.

#### CRediT authorship contribution statement

**Liangfu Ge:** Conceptualization, Data curation, Formal analysis, Writing – original draft. **Ayan Sadhu:** Funding acquisition, Project administration, Supervision, Writing – review & editing.

#### Declaration of competing interest

The authors declare that they have no known competing financial interests or personal relationships that could have appeared to influence the work reported in this paper.

#### Data availability

Data will be made available on request.

#### Acknowledgments

The authors would like to acknowledge the financial support through the Discovery Grant of the Natural Sciences and Engineering Research Council (NSERC) of Canada and the Early Researcher Award funding provided by the Ontario Ministry of Colleges and Universities to the corresponding author. The authors also acknowledge the Western Academy for Advanced Research (WAFAR) of Western University for their financial support through the Western Fellowship and Postdoctoral Fellowship to the corresponding author and the first author, respectively. Also, the authors thank Dr. Brownjohn and Dr. Koo from the University of Exeter for their support on the steel beam experiments.

#### References

- [1] W.-X. Ren, H.-B. Chen, Finite element model updating in structural dynamics by using the response surface method, *Eng. Struct.* 32 (8) (2010) 2455–2465.
- [2] R. Ferrari, D. Froio, E. Rizzi, C. Gentile, E.N. Chatzi, Model updating of a historic concrete bridge by sensitivity-and global optimization-based Latin Hypercube Sampling, *Eng. Struct.* 179 (2019) 139–160.
- [3] J. Mao, H. Wang, J. Li, Bayesian finite element model updating of a long-span suspension bridge utilizing hybrid Monte Carlo simulation and kriging predictor, *KSCE J. Civ. Eng.* 24 (2) (2020) 569–579.
- [4] M. Mishra, Machine learning techniques for structural health monitoring of heritage buildings: A state-of-the-art review and case studies, *J. Cult. Herit.* 47 (2021) 227–245.
- [5] S.S. Afshari, F. Enayatollahi, X. Xu, X. Liang, Machine learning-based methods in structural reliability analysis: A review, *Reliab. Eng. Syst. Saf.* 219 (2022) 108223.
- [6] S. Sony, K. Dunphy, A. Sadhu, M. Capretz, A systematic review of convolutional neural network-based structural condition assessment techniques, *Eng. Struct.* 226 (2021) 111347.
- [7] L. Ge, K.Y. Koo, M. Wang, J. Brownjohn, D. Dan, Bridge damage detection using precise vision-based displacement influence lines and weigh-in-motion devices: Experimental validation, *Eng. Struct.* 288 (2023) 116185.
- [8] P. Sevdentekidis, D. Giagopoulos, A. Arailopoulos, O. Markogiannaki, Structural Health Monitoring using deep learning with optimal finite element model generated data, *Mech. Syst. Sig. Process.* 145 (2020) 106972.
- [9] S. Sony, S. Gamage, A. Sadhu, J. Samarabandu, *Vibration-based multiclass damage detection and localization using long short-term memory networks. Structures*, Elsevier, 2022.
- [10] S. Sony, S. Gamage, A. Sadhu, J. Samarabandu, Multiclass damage identification in a full-scale bridge using optimally tuned one-dimensional convolutional neural network, *J. Comput. Civ. Eng.* 36 (2) (2022) 04021035.
- [11] M. Zhao, A. Sadhu, M. Capretz, Multiclass anomaly detection in imbalanced structural health monitoring data using convolutional neural network, *J. Infrastruct. Preserv. Resil.* 3 (1) (2022) 10.
- [12] Z.-Q. Yuan, Y. Xin, Z.-C. Wang, Y.-J. Ding, J. Wang, D.-H. Wang, Y. Yang, Structural nonlinear model updating based on an improved generative adversarial network, *Struct. Control Health Monit.* 2023 (2023) 1–21.
- [13] S. Teng, X. Chen, G. Chen, L. Cheng, Structural damage detection based on transfer learning strategy using digital twins of bridges, *Mech. Syst. Sig. Process.* 191 (2023).
- [14] Z. Zhang, C. Sun, Structural damage identification via physics-guided machine learning: a methodology integrating pattern recognition with finite element model updating, *Struct. Health Monit.* 20 (4) (2020) 1675–1688.

- [15] Z. Zhang, C. Sun, B. Guo, Transfer-learning guided Bayesian model updating for damage identification considering modeling uncertainty, *Mech. Syst. Sig. Process.* 166 (2022).
- [16] R. Wang, J. Li, S. An, H. Hao, W. Liu, L. Li, Densely connected convolutional networks for vibration based structural damage identification, *Eng. Struct.* 245 (2021) 112871.
- [17] T. Zhang, Y. Wang, Deep learning algorithms for structural condition identification with limited monitoring data, in: International Conference on Smart Infrastructure and Construction 2019 (ICSIC), 2019, pp. 421–426.
- [18] N. Bao, T. Zhang, R. Huang, S. Biswal, J. Su, Y. Wang, Y.-J. Cha, A deep transfer learning network for structural condition identification with limited real-world training data, *Struct. Control Health Monit.* 2023 (2023) 1–18.
- [19] P. Singhal, R. Walambe, S. Ramanna, K. Koticha, Domain adaptation: challenges, methods, datasets, and applications, *IEEE Access* 11 (2023) 6973–7020.
- [20] L.A. Gardner, J. Bull, N.D. Gosliga, K. Worden, Foundations of population-based SHM, Part III: Heterogeneous populations – Mapping and transfer, *Mech. Syst. Sig. Process.* 149 (2021).
- [21] L.A. Gardner, N.D. Bull, K. Worden, Domain-adapted Gaussian mixture models for population-based structural health monitoring, *J. Civil Struct. Health Monit.* 12 (6) (2022) 1343–1353.
- [22] Wang, Y. Xia, Knowledge transfer for structural damage detection through re-weighted adversarial domain adaptation, *Mech. Syst. Sig. Process.* 172 (2022).
- [23] Z. Chen, C. Wang, J. Wu, C. Deng, Y. Wang, Deep convolutional transfer learning-based structural damage detection with domain adaptation, *Appl. Intell.* (2022).
- [24] P. Martakis, Y. Reuland, A. Stavridis, E. Chatzi, Fusing damage-sensitive features and domain adaptation towards robust damage classification in real buildings, *Soil Dyn. Earthq. Eng.* 166 (2023).
- [25] F. Luleci, F.N. Catbas, O. Avci, A literature review: Generative adversarial networks for civil structural health monitoring, *Front. Built Environ.* 8 (2022) 1027379.
- [26] F. Luleci, F.N. Catbas, A brief introductory review to deep generative models for civil structural health monitoring, *AI Civil Eng.* 2 (1) (2023) 9.
- [27] F. Luleci, & Catbas, Condition transfer between prestressed bridges using structural state translation for structural health monitoring, *AI Civil Eng* 2 (1) (2023) 7.
- [28] Luleci, F. Necati Catbas, O. Avci, CycleGAN for undamaged-to-damaged domain translation for structural health monitoring and damage detection, *Mech. Syst. Sig. Process.* 197 (2023).
- [29] F. Luleci, A. Onur, F.N. Catbas, Improved undamaged-to-damaged acceleration response translation for Structural Health Monitoring, *Eng. Appl. Artif. Intel.* 122 (2023).
- [30] F. Gatti, L. Rosafalco, G. Colombera, S. Mariani, A. Corigliano, Multi-storey shear type buildings under earthquake loading: Adversarial learning-based prediction of the transient dynamics and damage classification, *Soil Dyn. Earthq. Eng.* 173 (2023) 108141.
- [31] X. Pan, C. Ge, R. Lu, S. Song, G. Chen, Z. Huang, G. Huang, On the integration of self-attention and convolution. Proceedings of the IEEE/CVF conference on computer vision and pattern recognition, 2022.
- [32] Y. Liu, G. Sun, Y. Qiu, L. Zhang, A. Chhatkuli, L. Van Gool, Transformer in convolutional neural networks. *arXiv preprint arXiv:2106.03180*, (2021) 3.
- [33] I. Goodfellow, J. Pouget-Abadie, M. Mirza, B. Xu, D. Warde-Farley, S. Ozair, Y. Bengio, Generative adversarial networks, *Commun. ACM* 63 (11) (2020) 139–144.
- [34] A. Radford, L. Metz, S. Chintala, Unsupervised representation learning with deep convolutional generative adversarial networks. *arXiv preprint arXiv: 1511.06434*, (2015).
- [35] A. Brock, J. Donahue, K. Simonyan, Large scale GAN training for high fidelity natural image synthesis. *arXiv preprint arXiv:1809.11096*, (2018).
- [36] T. Karras, S. Laine, T. Aila. A style-based generator architecture for generative adversarial networks. In: *Proceedings of the IEEE/CVF conference on computer vision and pattern recognition*. (2019).
- [37] E.L. Denton, S. Chintala, R. Fergus, Deep generative image models using a laplacian pyramid of adversarial networks, *Adv. Neural Inf. Proces. Syst.* 28 (2015).
- [38] J.-Y. Zhu, P. Krähenbühl, E. Shechtman, A.A. Efros, Generative visual manipulation on the natural image manifold. *Computer Vision–ECCV 2016: 14th European Conference, Amsterdam, the Netherlands, October 11–14, 2016, Proceedings, Part V 14*, Springer, 2016.
- [39] P. Isola, J.-Y. Zhu, T. Zhou, A.A. Efros, Image-to-image translation with conditional adversarial networks. *Proceedings of the IEEE conference on computer vision and pattern recognition*, 2017.
- [40] J.-Y. Zhu, T. Park, P. Isola, A.A. Efros, Unpaired image-to-image translation using cycle-consistent adversarial networks. *Proceedings of the IEEE international conference on computer vision*, 2017.
- [41] A. Vaswani, N. Shazeer, N. Parmar, J. Uszkoreit, L. Jones, A.N. Gomez, I. Polosukhin, Attention is all you need, *Adv. Neural Inf. Proces. Syst.* 30 (2017).
- [42] A.L. Maas, A.Y. Hannun, A.Y. Ng, Rectifier nonlinearities improve neural network acoustic models. *Proc. icml*, 2013. Atlanta, GA.
- [43] I. Loshchilov, F. Hutter, Decoupled weight decay regularization. *arXiv preprint arXiv:1711.05101*, (2017).
- [44] C. Krämer, C. De Smet, B. Peeters, Comparison of ambient and forced vibration testing of civil engineering structures. *Proceedings of IMAC*, 1999.
- [45] Z. Shang, Y. Xia, L. Chen, L. Sun, Damping ratio identification using attenuation responses extracted by time series semantic segmentation, *Mech. Syst. Sig. Process.* 180 (2022).
- [46] X. Ling, A. Haldar, Element level system identification with unknown input with Rayleigh damping, *J. Eng. Mech.* 130 (8) (2004) 877–885.
- [47] E. Reynuers, System identification methods for (operational) modal analysis: review and comparison, *Arch. Comput. Meth. Eng.* 19 (2012) 51–124.